MultiSoft: Soft Sensor Enabling Real-Time Multimodal Sensing with Contact Localization and Deformation Classification

SANG HO YOON, Purdue University, USA
LUIS PAREDES, Purdue University, USA
KE HUO, Purdue University, USA
KARTHIK RAMANI, Purdue University, USA

We introduce *MultiSoft*, a multilayer soft sensor capable of sensing real-time contact localization, classification of deformation types, and estimation of deformation magnitudes. We propose a multimodal sensing pipeline that carries out both inverse problem solving and machine learning tasks. Specifically, we employ an electrical impedance tomography (EIT) for contact localization and a support vector machine (SVM) for classifying deformations and regressing their magnitudes. We propose a deformation-aware system which enables maintaining a persistent single-point contact localization throughout the deformation. By updating a time-varying distribution of conductivity change caused by deformations, a single-point contact localization can be maintained and restored to support interaction using both contact localization and deformations. We devise a multilayer structure to fabricate a highly stretchable and flexible soft sensor with a short sensor settlement after excitations. Through a series of experiments and evaluations, we validate both raw sensor and multimodal sensing performance with the proposed method. We further demonstrate applicability and feasibility of *MultiSoft* with example applications.

CCS Concepts: • **Human-centered computing** → Interaction devices; Interaction techniques; • **Hardware** → Sensors and actuators; Tactile and hand-based interfaces;

Additional Key Words and Phrases: Soft user interface, wearables, input device, sensing technique, multimodal sensing

ACM Reference Format:
Sang Ho Yoon, Luis Paredes, Ke Huo, and Karthik Ramani. 2018. MultiSoft: Soft Sensor Enabling Real-Time Multimodal Sensing with Contact Localization and Deformation Classification. *Proc. ACM Interact. Mob. Wearable Ubiquitous Technol.* 2, 3, Article 145 (September 2018), 21 pages. https://doi.org/10.1145/3264955

1 INTRODUCTION

Recent advancements in electronic hardware and signal processing techniques have enabled new types of sensing capabilities. Recent works have shown unique capabilities using acoustic, capacitive, piezoelectric, and bioimpedance sensing [19, 28, 31, 32]. With these versatile sensing capabilities, a wide range of interactions, from touch sensing [50] to deformation sensing [41], has been investigated. However, providing multimodal sensing is difficult in two aspects: 1) software is generally tuned for supporting single sensing modality and 2) hardware is typically limited to inherent physical sensing capability (e.g. either pressure or strain sensing). To improve both software and hardware aspects, we propose a multimodal sensing pipeline using an enhanced soft sensor structure.

Authors' addresses: Sang Ho Yoon, Purdue University, West Lafayette, IN, 47907, USA, yoon87@purdue.edu; Luis Paredes, Purdue University, West Lafayette, IN, 47907, USA, lparede@purdue.edu; Ke Huo, Purdue University, West Lafayette, IN, 47907, USA, khuo@purdue.edu; Karthik Ramani, Purdue University, West Lafayette, IN, 47907, USA, ramani@purdue.edu.

2474-9567/2018/9-ART145 $15.00
https://doi.org/10.1145/3264955

To interpret users' inputs from sensor signals, two general approaches have been studied: 1) solving specific inverse problem or 2) utilizing machine learning. A sensing system that solves inverse problems exhibits a high accuracy where no training process is required. But in cases of the system containing large number of sensing nodes along with non-linear sensing characteristics, the pattern of sensor values becomes too complex to be formulated as an inverse problem. To this end, recent works started to adopt machine learning algorithms to model complex patterns of sensor values [10, 41, 50]. On the other hand, an ad-hoc training infused learning-based approach has shown strong potential for interpreting users' inputs from multi-dimensional sensor readings. A recent work [25] has incorporated machine learning algorithms with heuristics to explain both surface and deformation gestures. To this end, we leverage both approaches and propose a multimodal sensing pipeline for a soft sensor. The proposed pipeline adopts an inverse problem solver (EIT) for localizing contact and a machine learning algorithm (SVM) for classifying a deformation type as well as a magnitude.

With the development of soft materials, recent works have transformed the form factor of the sensor from a rigid body to a soft [45], flexible [33], stretchable [47], and conformable [46] body. With this freedom from a rigidity, these works have introduced various types of input sensing including touch, pressure, bend, and squeeze to both soft and rigid substrates. However, a specific sensor design is required for each different sensing modality and a pre-defined sensor design is needed to provide a contact localization. In this work, we propose a soft sensor that does not require a pre-defined sensor design for locating a contact point while supporting learning on deformation types and intensities.

We employ a non-toxic piezoresistive carbon-filled elastomer [44] which has been widely used for providing various sensing methods. A slow recovery and a small baseline shift of sensing signals after excitations make it hard to support real-time localization as well as training deformation behaviors. We previously explored the soft sensor with two sensing modalities including a real-time contact localization (locating a contact point) and stretching sensing separately [49]. Furthermore, another work focused on providing a robust contact localization on a stretchable sensor [3]. However, to fully support a natural interaction cycle (i.e. contact-hold-stretch-recover-release), we need to accurately detect the deformations caused by different interactions. Moreover, recognizing different types and magnitudes of the deformation are also limited by the previous sensor structure and sensing algorithm [49]. To support various deformations, we made breakthroughs in our deformation-aware sensing pipeline, sensor structure, fabrication process, and system flow.

To this end, we introduce a multilayer sensor structure to enhance physical properties as well as fabrication conditions. We further apply dynamic manipulation to encourage fast sensor settlement to enable a robust training for deformation behaviors. Moreover, we employ a deformation state machine to form a sensing pipeline to maintain a persistent single-point contact localization during and after the presence of deformations. This allows us to provide meaningful interaction such as combining contact localization with various deformations.

In this work, we introduce *MultiSoft*, which enables a real-time multimodal sensing with a multilayer soft sensor. We employ a multimodal sensing pipeline where localization is computed with an EIT image reconstruction while different types and magnitudes of deformations are classified with a trained SVM classifier and regression models. Using a low-cost soft sensor, we empower users to perform interactions that support natural motions and behaviors which cannot be accommodated with a single sensing modality. Our contributions are as follows:

- Contact localization while recognizing different types and magnitudes of deformations
- A multimodal sensing pipeline to maintain a single-point contact localization through deformations
- A multilayer sensor structure that enhances physical properties as well as the sensor settling time
- Example applications demonstrating the use of the multimodal sensing capability of *MultiSoft*

2 RELATED WORK

2.1 Sensing Modality

Different types of mechanical strains have been utilized for various input sensing modalities including pressure [6, 9, 27], shear [21, 30], bending [8, 24, 37], and stretching [39, 43]. The expanded sensing modalities enable the use of natural motions such as stretching textiles and bending flexible objects as an input metaphor. To this extent, a variety of applications have been suggested in HCI contexts such as a jamming/squeezable/pinching interface [11], a wearable gesture recognition [10], gaming [35], and smart textiles [7, 22, 26]. Furthermore, recent works [25, 48] have incorporated distinct sensing modalities as a single form of sensor to enrich the capability of the input sensing. In [25], a hybrid gesture detection pipeline containing machine learning along with heuristics enables surface and deformation gesture detection. In our work, we suggest a method to enable multimodal sensing that includes localization, deformation classification, and deformation level estimation.

2.2 Soft Sensors in HCI

Recent applications of advanced materials have enabled sensing with soft [37, 45], stretchable [39, 47], and flexible materials [8, 28]. Utilizing these sensing methods, HCI researchers have supported diverse form factors including a tattoo skin [16], flexible objects [33], and soft-matters [49]. This wide applicability in embedding sensing capability into various surfaces requires a quick understanding of complex sensor values. Still, the soft sensor needs to be designed beforehand to support designated applications and it requires time and cost to change the whole design. For these reasons, researchers have worked on approaches that can bring down the cost of making soft sensors [45, 47] along with high customization capabilities [49]. Our approach is aligned with these directions: We propose a sensing pipeline that can instantly support contact localization and deformation sensing without the need for major design changes. We also ease the fabrication condition with reduced curing temperature and duration. And we improve the sensor settlement after excitations through a multilayer sensor structure based on highly stretchable silicone.

2.3 Electrical Impedance Tomography for Input Sensing

Electrical impedance tomography (EIT) has been implemented widely in robotics and HCI fields to provide various input sensing. In particular, the EIT approach has enabled tactile sensing [2] and hand gesture recognition [51] without distributed sensory elements in the sensing area. This frees the sensors from complex wirings and allows sensing with a single-volume material. To further expand the interaction capability, EIT has shown promise for sensing the modality of touch [36], multi-directional strain [21], and touch sensing on arbitrary surfaces [50]. A recent work has showcased real-time continuous contact localization with a soft material [49]. However, the ability to support and restore contact localization upon and after deformation is still challenging. By utilizing the benefits from a deformation-aware system, we preserve the EIT based contact localization performance upon/after deformation.

2.4 Sensing Technique Method

A system that follows general theories or known behaviors supports a high accuracy and robustness by solving a specific problem. For instance, EIT solver algorithms are built from efficient and reliable mathematical models which directly reflect a physical relationship between variables (voltage readings) and the output (resistance distribution) [2]. However, such mathematical models are usually constrained by certain assumptions. For the EIT solver, the sensors' planar surface is assumed not to be deformed. For other use cases, however, there are no concise mathematical models that especially consider practical uncertainties such as complex behaviors, user-dependencies, and non-linearities. To this end, machine learning algorithms provide definite solutions as they rely on a training dataset without using any explicit model. Recent works have also shown the robustness of

the machine learned model for understanding/recognizing user inputs with wearables [10], deformations [41], a configuration of hands [31], arbitrary surface [50], and multiple sensors [20]. In our work, we aim to combine the benefits of EIT for contact localization (user independent) and SVM for understanding deformation (more user-dependent).

Our current work directly extends from iSoft [49] which utilizes a soft piezoresistive material along with a capacitive sensing to provide a real-time contact localization as well as a stretch sensing. In this work, we expand the interaction potentials of previous work in a new domain by classifying different sensing modalities and detecting their intensities. We propose a multilayer sensor structure and a new fabrication process which supports sensing various deformations. We also develop a multimodal sensing pipeline which enables a new kind of interaction cycle such as the combination of contact localization along with deformation (i.e. touch-stretch-release interaction). In this work, we introduce a low-cost approach so that the researchers and practitioners can explore the soft sensor with multiple sensing modalities.

3 DESIGN CHALLENGES AND GOALS

Contact Localization with Deformation: We aim to support multimodal sensing that accommodates natural human motions and behavior. To achieve this, our proposed multimodal sensing pipeline should maintain contact localization (local deformation) upon and after global deformation. Here, global deformation refers to any deformation that causes high strain changes in overall sensing regions (i.e., stretching & bending). Throughout the chapter, we refer to global deformation as *deformation*. It is not common for humans to continuously move their fingertips during deformation. Thus, we utilize the contact localization information before the deformation for maintaining and restoring the localization during and after the deformation.

Interactions with Soft Sensors: With the stretchable and flexible nature of soft sensors, the sensing technique should support expanded input vocabulary utilizing its physical properties. Understanding deformations can contribute to this goal in which various deformation types (stretching, bending, squeezing, pressing, etc.) are potential candidates for interactions with the soft sensor. Furthermore, the rich information regarding deformation (e.g., level of intensity) would enable additional dimensions to the existing input metaphor.

Fabrication & Form Factor: Low cost and less setup are desirable for sensor fabrication. Specifically, low temperature and short curing duration conditions can reduce the equipment cost as well as the applicability of embedding sensors into various materials and objects. In terms of performance, highly flexible and stretchable sensors that are free from sensor settlement after excitation would be ideal. In this chapter, we emphasize making soft sensors that can easily be attached to objects or used as a wearable device.

4 MULTILAYER SENSOR FABRICATION

Design Rationale & Fabrication Process: Our fabrication employs a multilayer approach where we used platinum cure liquid silicone as our base substrate. Using a multilayer structure has several advantages: 1) providing repeatable signal patterns and magnitudes to help classifying deformation types and intensities, 2) enhancing the user comfort by providing a highly stretchable form factor, 3) more deployable by reducing the curing temperature/duration while supporting conformable attachment to various substrates in room temperature, and 4) improving strain sensitivity.

As shown in Figure 1 (A)~(C), we started with making the base substrate by pouring platinum cure liquid silicone compounds onto a laser-cut plastic mold. In this study, we fabricated different mold sizes: width between 5~15 cm, length between 5~20 cm, and thickness between 0.8~2.5 mm. The liquid silicon was cured at 25°C for either 30 or 75 minutes according to the selected Dragon Skin® [38] product specifications. We used a product with a short pot life (4 minutes) for smaller mold (<100 cm^2) and longer pot life (8 minutes) for larger mold. Then, we applied carbon-filled rubber on top of the cured base substrate using a painting knife as recommended

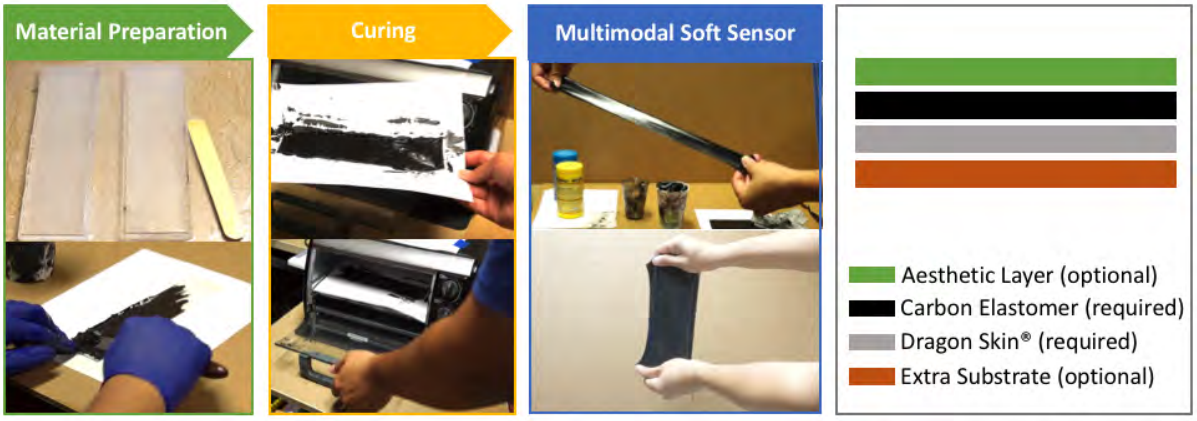

Fig. 1. *MultiSoft* fabrication process: (A) Preparing highly stretchable silicone base with mold and paint carbon-filled elastomer over cured base and (B) curing the substance with a toaster oven at 65°C for 10 minutes. This produces (C) highly flexible and stretchable soft sensors for multimodal sensing and (D) *MultiSoft* layer structure.

in [40]. By applying a carbon-filled rubber as a thin substrate (<0.5 *mm*), curing requirements for temperature and duration came down to 65°*C* for 10 minutes comparing to 165°*C* for 15 minutes to cure a single-volume sensor [49]. We confirmed that our fabrication process is also scalable by fabricating with existing preprocessed silicone elastomer film (Elastosil® Film [44] with thickness of 0.2~0.4 *mm*). Figure 1 (D) represents the layer structure of the proposed soft sensor.

Material & Equipment: Our core material is carbon-filled silicone rubber from Wacker Ltd. [44], which has a volume resistivity (11 Ω·*cm*) similar to that of carbon nanotube based polymer sensors (1~200 Ω·*cm*), but lower cost. We also used very soft, highly stretchable platinum cure liquid silicone compounds (Dragon Skin®) which can be stretched up to more than 500% without rupture. The curing of carbon-filled silicone rubber can be done using a toaster oven (< $50) in which the curing condition is 10 minutes at 65°C. Heat stabilized film ($1.7/letter-size sheet) can be used to produce smooth sensor surfaces. Without the film, we observed that it was hard to control the surface roughness of the cured elastomer because of its high viscosity. The current cost of making a letter-sized sensor is about $6~10 for a thickness of between 0.8 and 2.5 *mm*.

5 SENSING APPROACH

Figure 2 illustrates our sensing boards. The dimensions of the sensing boards are 5(W)×5(L) *cm* (16-Channel). For the electrodes, we used ribbon crimp end since it provided a firm contact with quick installation. Wires were soldered on the crimp end to provide a connection between the board and the sensor.

5.1 Hardware & Data Acquisition

As shown in Figure 2, our customized 16-channel shield was equipped with Teensy board (MK20DX256VLH7) [15]. The general components included an adjustable current source (LM334, Texas Instruments) and an instrumentation amplifier (AD623, Analog Devices). A total of four 16-to-1 (CD74HC4067, Texas Instrument) multiplexers were used to implement the switching matrix according to the required number of channels. The total cost of the board was $30 (16-channel). The current size and cost are an upper limit which can be further reduced with commercial production.

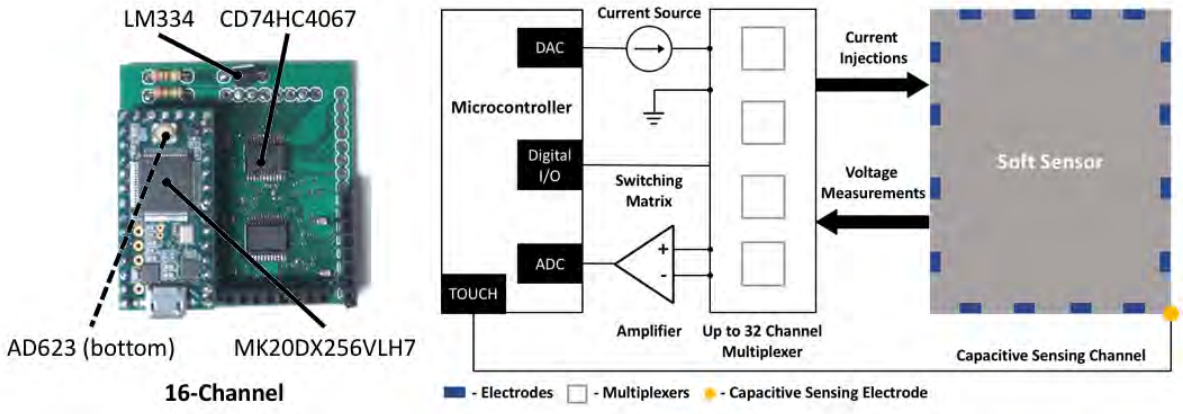

Fig. 2. 16-channel customized sensing board (Left) and schematic view of our system (Right).

Figure 2 presents a schematic view of our prototype. We adopted a neighboring method which has been used as a robust pooling method in previous works [49, 51]. The system underwent a two-step process including voltage measurement and capacitive sensing. First, a small current (0.5 mA) was injected and voltages were measured after the current propagation (100 μs delay). After the voltage measurement cycle, a capacitive reading was performed with a designated Touch Pin from Teensy, which utilized a microcontroller's internal capacitance (<100 μs). The maximum sampling rate for pooling 16 channels was 60 Hz.

5.2 Resistance Measurement Method

The core sensor values are based on real-time resistance distribution along the material, which changes upon external mechanical strains caused by contact pressure, stretching, and bending. As shown in Figure 3, we employed a four-terminal sensing, which reduced the inaccuracy from the variance in contact resistance. The electrodes were placed surrounding the objects, and we adopted the *Neighboring Method* which injected DC current into two adjacent electrodes. Also, a number of voltage measurements were done on successive adjacent

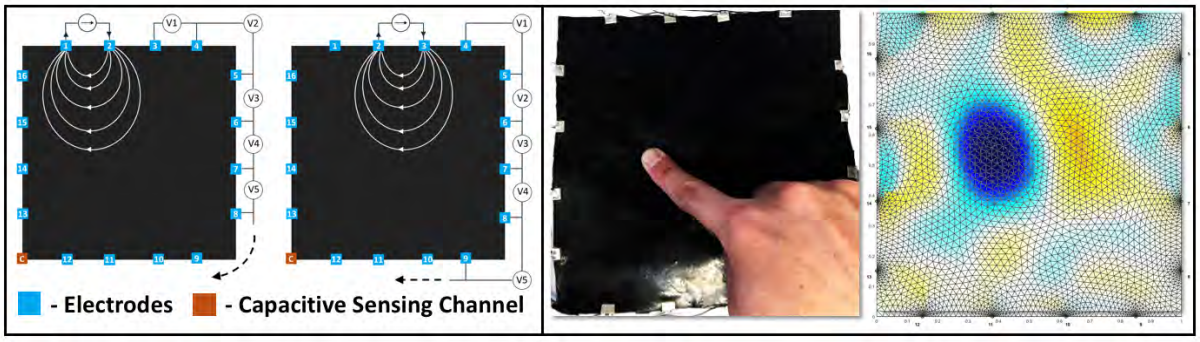

Fig. 3. Four-terminal sensing employing the Neighboring Method with a capacitive sensing channel (Left). EIT technique based tracking workflow using a Finite Element Model and an image reconstruction (Right).

electrode pairs as illustrated in [4]. With 16 electrodes, this resulted in a total number of 208 voltage measurements. We fed the same raw sensor values into EIT and SVM channels in the multimodal sensing pipeline.

5.3 Contact Localization & Deformation Sensing

The implemented contact localization followed the method in [49] as shown in Figure 3. We used EIDORS EIT Toolkit [42] where a regularized maximum a posteriori [1] using one step Gauss Newton solver was applied to the four-step image reconstruction: 1) a pre-computation (< 3*s*), 2) a single matrix computation with resistance changes (2.5 *ms*), 3) an image reconstruction (25 *ms*), and 4) a color filter for computing the effective region's centroid (0.5 *ms*). The frame rate of the EIT image reconstruction was 35 Hz with a 16-electrode configuration.

For the deformation sensing, we used a Support Vector Machine (SVM), and for the input features, we only used raw voltage measurements with no additional data modifications. Thus, the length of our feature set was 208 voltage readings (16-channel). We used a Weka toolkit [13] to perform SVM (SMO, Polykernel with E=1.0) for deformation classification and SVM regression (SMOreg, Polykernel with E=1.0) to estimate the magnitude of the deformation. Multiple independent regression models were needed to support the magnitude estimation for multiple deformations (e.g., stretching in X and Y directions). For processing time, we observed less than 15 *ms* (> 65 Hz) to run one SVM model along with five SVM regression models. A linear classifier did not work well with the deformation classification due to the non-linear characteristics of the sensor response. Thus, we used a non-linear classifier. Overall, the current system computes the localization and deformation sensing in sequence, which yields a frame rate of 23 Hz using Macbook Pro (2.7 GHz).

6 MULTIMODAL SENSING PRINCIPLES

Our multimodal sensing is carried out both for the inverse problem solving (EIT) and machine learning (SVM) tasks. The changes in resistance distribution of the piezoresistive material provide sufficient information for understanding the deformation. With a deformation-aware system, we can correctly update the contact localization information in the presence of the deformation. The proposed approach allows us to maintain/restore contact localization during/after the deformation.

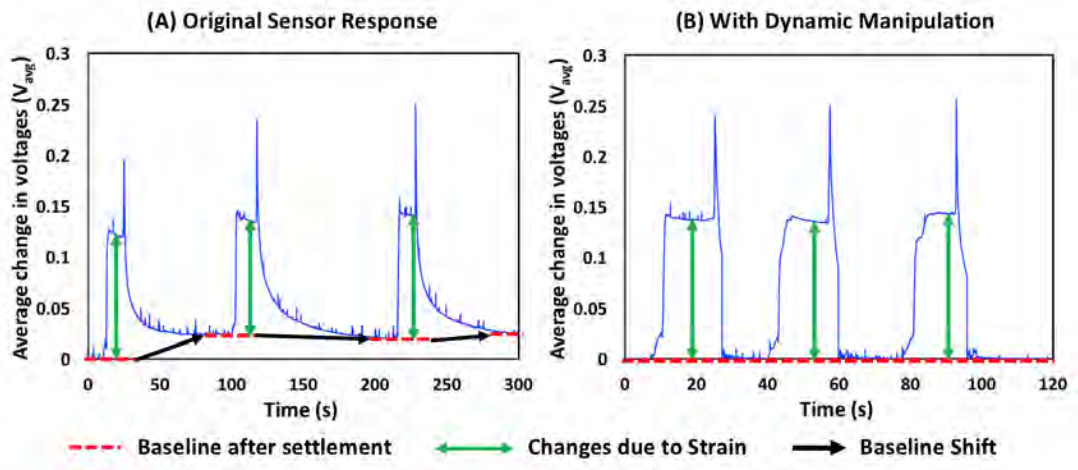

Fig. 4. Average change in all sensor values (A) without and (B) with dynamic manipulation upon applied strains.

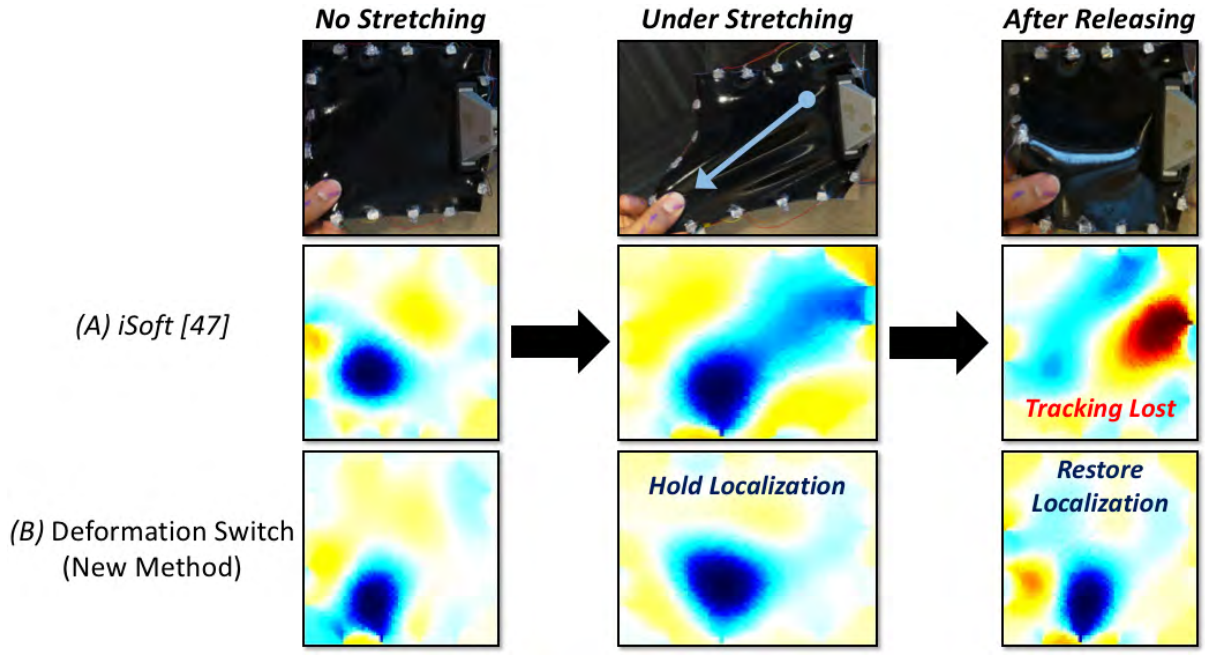

Fig. 5. Contact localization upon stretching. (A) Previous methods cannot maintain the localization due to a lack of deformation-awareness. (B) With a deformation switch, *MultiSoft* maintains contact localization during and after stretching.

Dynamic Manipulation: The carbon elastomer is known for non-linearity and long settlement after excitation. We captured several trials of uniform large stretching with existing carbon filled silicone as shown in Figure 4 (A), which shows a small baseline shift for each trial as well as a long settlement duration. Although we can learn the pattern behavior from the raw sensor values, this phenomenon can easily confuse the classifier. During our preliminary evaluation, the SVM classifier worked robustly if we kept the same zero level when there was no excitation. To maintain the zero level during the *No Deformation* state, we employed a calibration method for handling the temporal drift [14]. Here, we simply apply differential dynamic manipulation by setting the baseline of the sensor values to zero level when the sensor settlement enters into a quasi-steady state (Figure 4 (B)). The quasi-steady state is determined by looking at an average of discrete-time derivative of the changes in all the channels' sensor readings $d\mathbf{V}_{avg}$ (a running average of 10 frames) when an average change in all sensor values ($\mathbf{V}_{avg}$) is within a low strain range. Thus, the dynamic manipulation removes the temporal drift to enable the robust deformation training.

Deformation Switch: The EIT image reconstruction is processed with a difference in the resistance measurement ($\delta\mathbf{V}$), which is the difference between an instant measurement reading ($\mathbf{V}_i$) and the homogeneous baseline ($\mathbf{V}_H$). Previous work showed discrete contact sensing by taking a no-load condition as *a constant baseline* for computing the $\delta\mathbf{V}$ [2]. A real-time continuous contact localization was also introduced by updating the homogeneous baseline upon touch and movement [49]. Still, the EIT image reconstruction can easily deteriorate from the deformations due to resistance changes in the overall sensor region as shown in Figure 5(A).

We adopted a *deformation switch* to maintain and restore the contact localization upon deformation status. When deformation occurred, we kept the most recent $\delta\mathbf{V}$ before the deformation occurred. Then, this $\delta\mathbf{V}$ was maintained during the deformation. Upon release from the deformation, we restored the homogeneous baseline

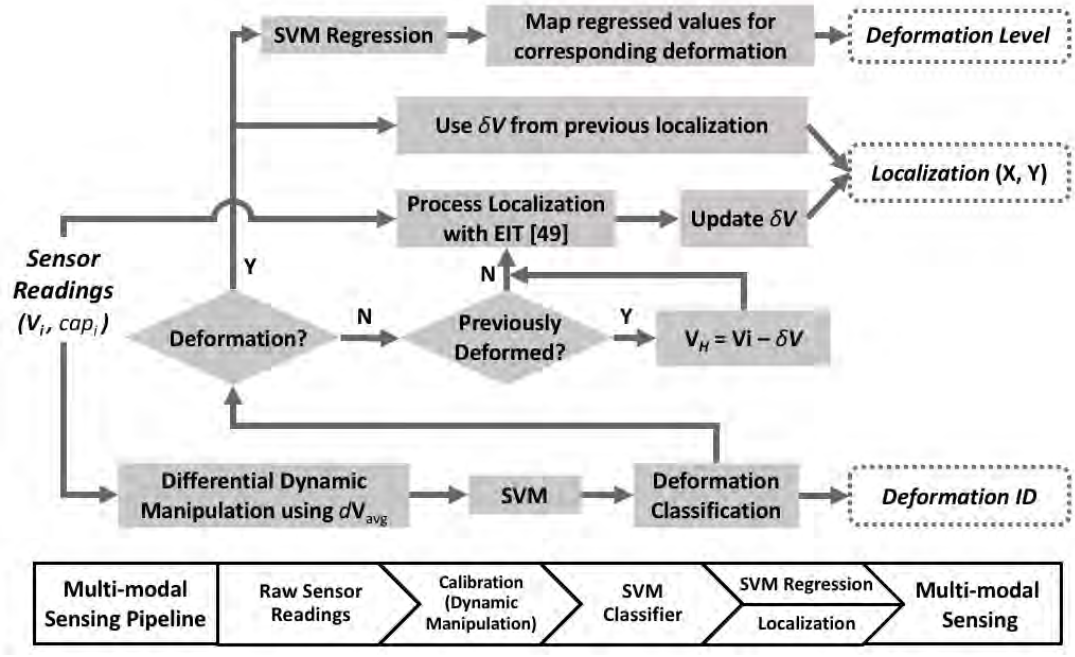

Fig. 6. System flow of multimodal sensing pipeline.

using $\delta\mathbf{V}$, where $\mathbf{V}_H = \mathbf{V}_i - \delta\mathbf{V}$. With the proposed method, the contact localization can be maintained during the deformation and restored after the deformation as shown in Figure 5(B).

With the aforementioned approaches, we achieved a multimodal sensing with contact localization and classification of the deformation (i.e., stretching & bending) type with magnitude. Figure 6 illustrates the detailed workflow of the system.

(1) Raw sensor readings ($\mathbf{V}_i$,cap_i) are fed into the EIT and SVM channels.
(2) Before feeding the sensor values to the SVM classifier, we apply differential dynamic manipulation when the sensor settlement enters the quasi-steady state, i.e., $d\mathbf{V}_{avg} < d\mathbf{V}_{avg,threshold}$ when $\mathbf{V}_{avg} < \mathbf{V}_{avg,threshold}$.
(3) We classify the deformation type using SVM with polynomial kernel.
(4) If the state becomes *No Deformation*, we confirm the presence of deformation in the previous frame.
(5) If a deformation event exists in the previous frame, we set $\mathbf{V}_H = \mathbf{V}_i - \delta\mathbf{V}$ to restore the homogeneous baseline. Otherwise, we process EIT localization using [49], update $\delta\mathbf{V}$ with current $\mathbf{V}_i$ and localize a contact coordinate.
(6) If any deformation is detected, multiple channels are activated: 1) we use $\delta\mathbf{V}$ from the most recent localization during *No Deformation* state and output a contact coordinate and 2) we determine the level of the corresponding deformation using SVM regression with polynomial kernel.

7 TECHNICAL FINDINGS

To understand the sensing capability of the proposed sensor, we investigated the attributes that affected the sensor performance. To be more specific, we evaluated the contact localization accuracy and the activation required

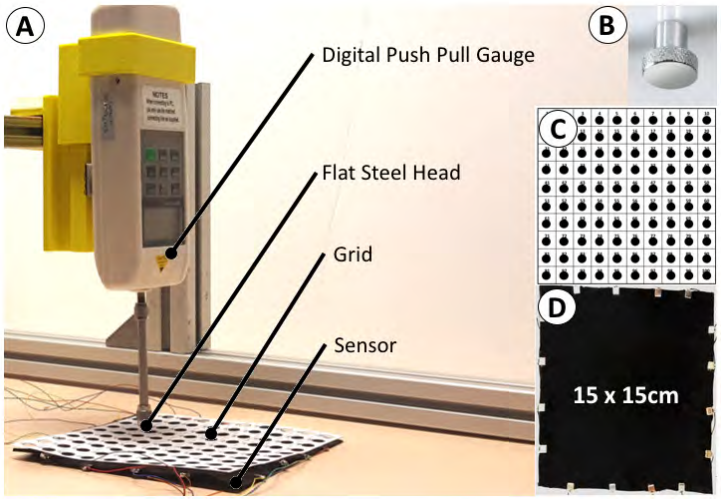

Fig. 7. (A) The overall test setup for localization accuracy and contact force requirement. (B) A flat steel head was selected to apply the pressure. (C) A 10 by 10 grid was used to test 100 different locations. (D) A 15×15 *cm* sensor was tested.

force. Then, we checked the pattern of the sensor values with different deformations and compared the sensor settlement after a large strain (> 40%).

7.1 Localization Accuracy & Contact Force Requirement

In this test, we evaluated the absolute distance error for the contact localization and force required to activate the sensor. Our main purpose was to compare these performances with [49] to confirm the feasibility of the proposed sensor for the contact localization as shown in Figure 7. The setup included a 15×15 *cm* multilayer sensor with 16-electrode configuration. We used a digital force gauge (HF-200) with a flat steel head for both evaluations.

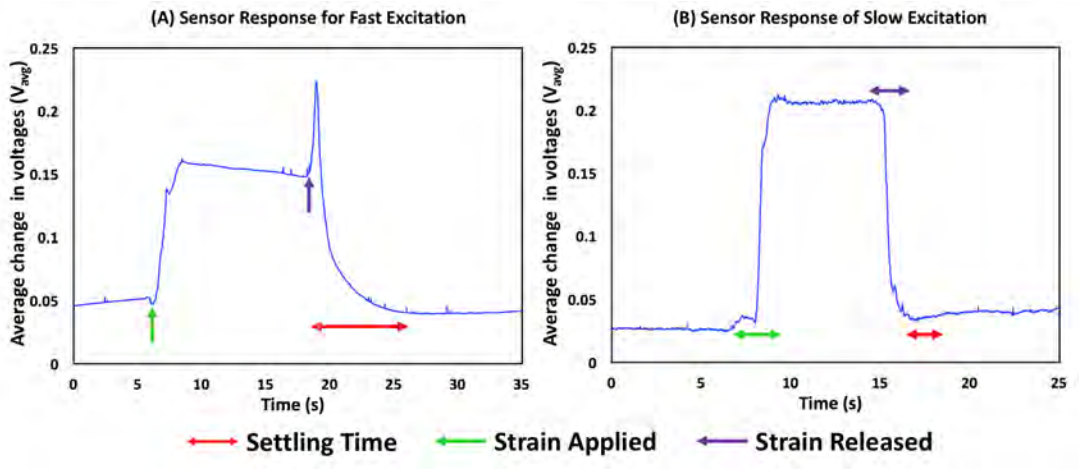

Fig. 8. Average change in voltage readings on a multilayer sensor upon > 40% strain with (A) fast and (B) slow excitations.

A 10×10 grid was used to dissect the sensor region for the evaluation. For the contact force measurement, the digital gauge logged the force when the contact sensing was activated.

The average targeting error came out to be 5.21 *mm* (SD=3.02) for *MultiSoft*. This error is similar to that of [49] in which the equivalent contact localization performance with the proposed multilayer fabrication was verified. On the other hand, the average contact force requirement was 1.55N (SD=0.46) with a range of 0.92~2.8N. The multilayer structure helped maintain a similar force requirement to that in prior work even with a thinner layer of the carbon-filled elastomer. The results confirmed that contact localization is feasible with the suggested prototype.

7.2 Sensor Settlement

We investigated the sensor settlement performance with the prototype. Previously, a single-volume carbon elastomer required a long sensor settling time (>10*s*) after excitation [23, 49]. We wanted to check how the settlement of the sensor changes with a multilayer structure that has a highly stretchable base. For the evaluation, we applied a stretch greater than 40% and released the sensor with both fast (Figure 8(A)) and slow (Figure 8(B)) excitations. We aimed to examine all possible behaviors of the proposed prototype since carbon-filled elastomer generally exhibits different characteristics under different excitation speeds of the applied strains. The required settling times were around 5s for fast excitations (<1*s*) and 2~3*s* for slow excitations (>3*s*). Thus, our fabrication process greatly improves the sensor settlement compared to in the previous sensor (>10*s*). Along with the proposed calibration using a dynamic manipulation, the proposed multilayer sensor can provide high repeatability. This would benefit the use of machine learning where the same pattern of sensor values is expected for the same deformation.

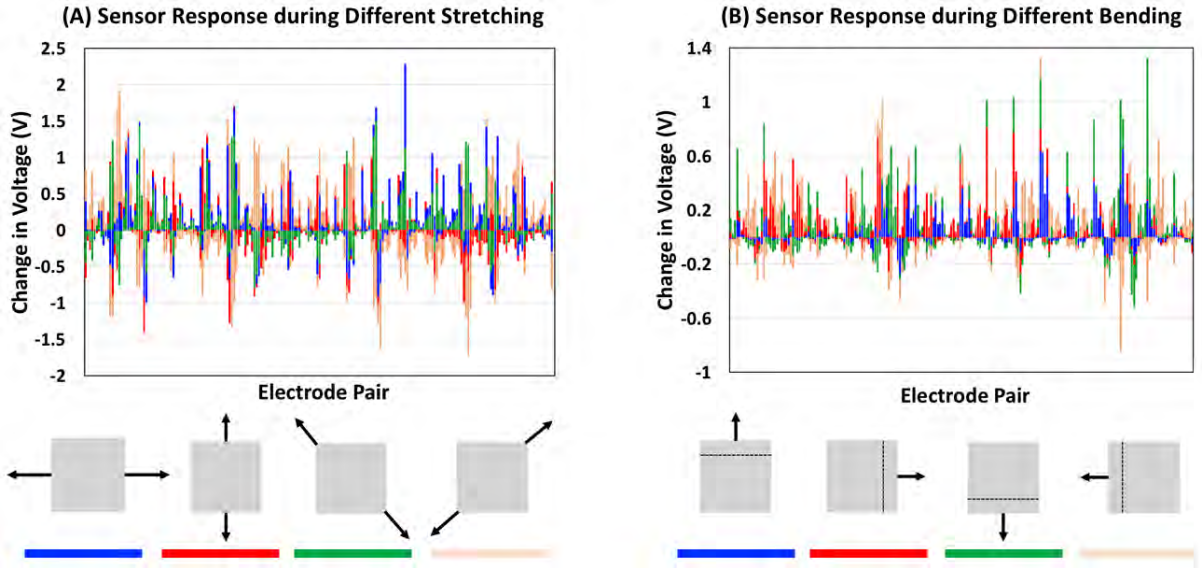

Fig. 9. Voltage measurements from all electrode pairs under different gestures for (A) Stretching and (B) Bending.

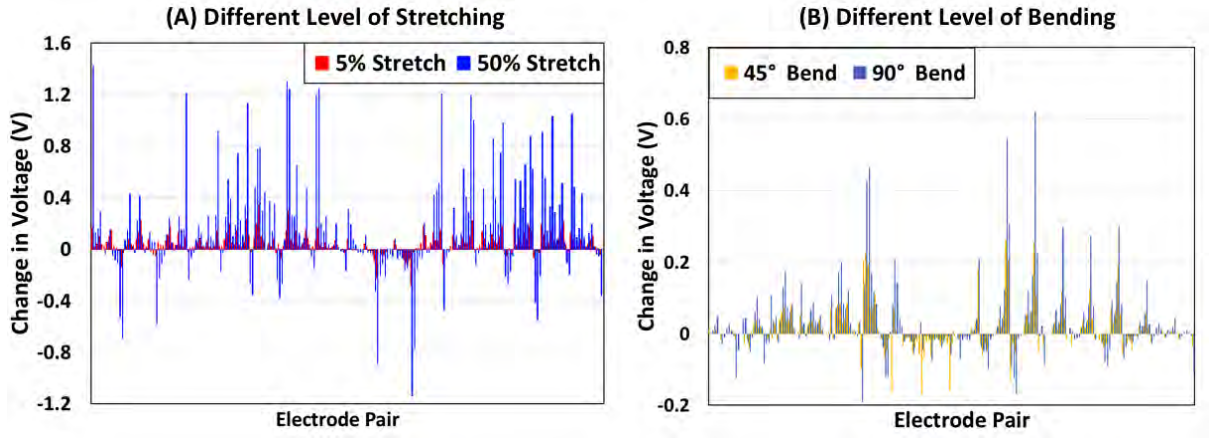

Fig. 10. Voltage measurements from all electrode pairs under different magnitudes of deformations for (A) Stretching and (B) Bending.

7.3 Signal Patterns with Deformations

For our machine learning model, we use the feature set that consists of a single frame of 208 raw voltage readings with a frame rate of greater than 30 Hz. We utilize these values to perform SVM and SVM regression to find out the type of deformation along with the level of deformation. Therefore, it is essential to check whether the sensor readings exhibit unique patterns upon distinct deformations and magnitudes. We especially explore this with stretching and bending since they cover deformations caused by both small (bending) and large (stretching) strains. Bending in mid-air will not produce any strain with the prototype. Also, we found out with a preliminary experiment that the sensor's base substrate should be greater than 0.8 *mm* in thickness due to insignificant sensor value changes upon bending. Therefore, we attach a 1 *mm*-thick fabricated sensor to a binder made with polypropylene for testing bending deformation.

We visualize a set of sensor readings for a single frame during different stretching (Figure 9(A)) and bending (Figure 9(B)) deformations. We can easily confirm from the visualization that each different deformation triggers a unique set of channels, but it is hard to find the overlapped sensor value pattern for different deformations. As expected, bending generally causes smaller changes in sensor values compared with stretching due to small strain changes. We also checked the sensor values in different magnitudes for the same deformation. As shown in Figure 10, we confirmed that the deformations with different magnitudes produce similar sensor value patterns except for their intensities. No difference was observed in terms of sensor value pattern for the same type of deformation. This confirms that the regression method can be employed for the magnitude estimation of deformations.

8 TASK EVALUATION

To verify the sensor performance with real users under controlled conditions, we divided the sensing workflow into three tasks: 1) contact localization accuracy during and after deformation, 2) accuracy of deformation classification, and 3) error rate of estimation on deformation magnitude. In all the evaluations, we used a 16-electrode configuration with a sensor size of 15×15 *cm*. For bending deformation, we used a prototype that is attached to a polypropylene binder similar to the one implemented in the **Technical Findings**. We recruited 15 participants (3 females) with a mean age of 29.

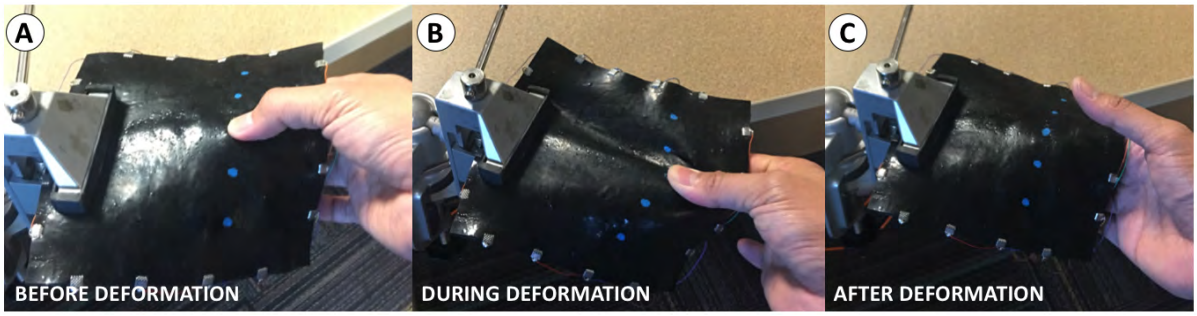

Fig. 11. The step-by-step process for testing localization accuracy upon deformation. (A) Users grasp painted target locations. (B) Users stretch the prototype while grasping the same target location for at least 2 *s* and (C) release the prototype.

8.1 Task 1: Localization Accuracy Under Deformation

We tested the robustness of our system in maintaining the contact localization in the presence of deformations. Our goal was to verify whether the persistent single-point contact localization worked correctly upon and after deformation using our approach.

Setup: We chose stretching as a representative deformation since stretching usually causes a large strain change in overall sensor regions compared to in other types of deformation. First, we trained a single baseline stretch for each participant where we recorded a single stretch instance on five different painted locations (Figure 11) to form a deformation switch. We evenly spaced painted locations along the sensor and placed them as close as possible to the center of the sensor while preventing sensors from being folded during grasping. If the deformation was not correctly classified during the contact accuracy evaluation, we excluded those trials since our aim was to check the robustness of the localization. The robustness of the deformation switch is verified in **8.2**. We asked users to grasp, stretch, and release on five different painted locations on the sensor. We averaged a total of at least 60 frames (20 frames for *Before*, *During*, and *After* deformations) for each trial. Here, we used *Before* deformation data as the ground truth for reporting the relative localization performance with *During* and *After* deformations. We divided the evaluation criteria into targeting accuracy (15×15 *mm* grid around the ground truth) and distance error. A total of 9000 data points was captured for the comparison (20 readings×3 instances×10 Trials×15 users).

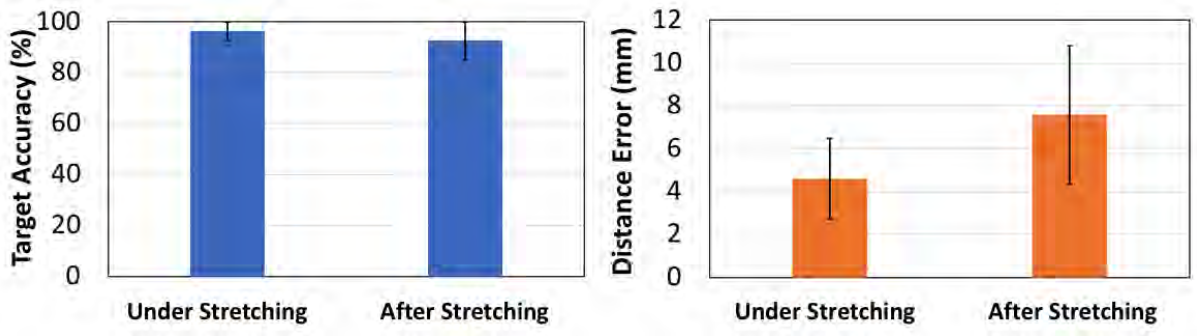

Fig. 12. Targeting accuracy (Left) and distance error (Right) of contact localization under and after stretching.

Result: As shown in Figure 12, participants maintained target accuracies of 96.4% and 92.7% and distance errors of 4.59 *mm* (SD=1.86) and 7.59 *mm* (SD=3.22) for *During* and *After Stretching*, respectively. The paired T-test showed no significant difference in targeting accuracy, but there was a significant difference ($p<0.05$) in distance errors. The small distance error in *Under Stretching* represents the robustness of the deformation switch for maintaining the contact localization. For *After Stretching*, we observed that the initial few frames (<10 frames) contributed heavily to the increased distance error. This suggests that we need to hold a few frames before re-initiating localization after releasing deformation. The results demonstrate that *MultiSoft* supports localization during deformation.

8.2 Task 2: Classification Accuracy

We evaluated the classification accuracy of various deformations with the SVM classifier. In our gesture sets, we included the reference gesture, which refers to holding the sensor with no stretching/bending. In this way, we could examine the robustness of the deformation switch while testing among the various gesture sets. We looked at the real-time classification accuracy of our prototype to see whether our deformation sensing is user-dependent or universal across users.

Setup: We divided our evaluation into two deformations (*Stretching* and *Bending*) with three different numbers of gesture set. We selected gestures that create the deformation in all directions as shown in Figure 13(C). The researcher recorded the raw sensor values when users performed the deformation. Participants held onto a visually instructed deformation for 1 *s* so the data could be captured. Also, the reference frame with no deformation was captured to check the robustness of deformation switch with various deformations. Here, we did not specify the detailed posture or the deformation intensity, which were solely the user's decision. We recorded the raw sensor values of 50 frames from each gesture for training purposes. Then we processed an N-class classifier for different numbers of gesture sets. Subsequently, we held a test session where we evaluated the classification accuracy *live*. Participants were asked to perform at least five trials of each gesture in a random order without repetitive gestures in a row. During the evaluation, we only used a per-user classifier to test the accuracy of the instant training, but we did keep records of the sensor values. For the post-hoc analysis, we processed a leave-one-user-out crossfold validation experiment to simulate the "Walk Up" (universal classifier) accuracy.

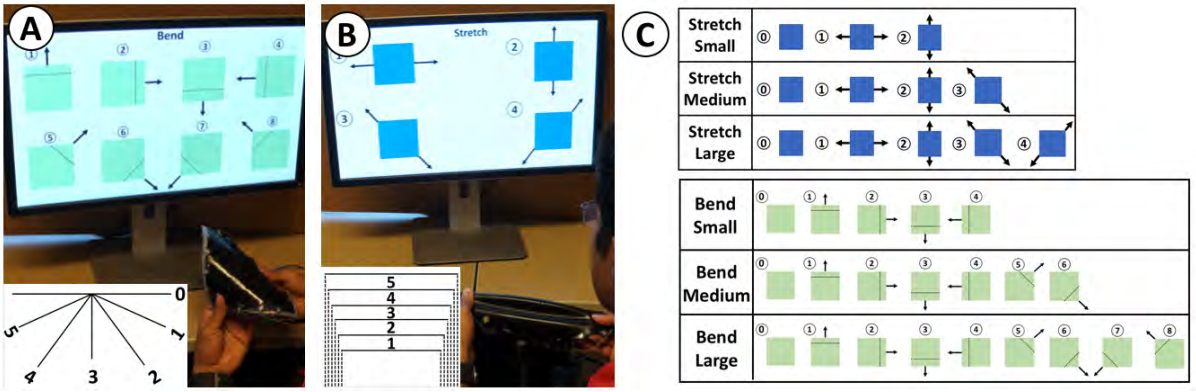

Fig. 13. The overall study setup for classification & regression accuracy for (A) bend, and (B) stretch gestures along with (C) corresponding gestures. Stretch gestures include stretching horizontally, vertically, and diagonally. Bend gestures include bending 1) upward, 2) right, 3) downward, 4) left, 5) top-right, 6) bottom-right, 7) bottom-left, and 8) top-left. Reference gesture (gesture '0' in the table) is also recorded when users just hold onto the sensor without any stretching or bending.

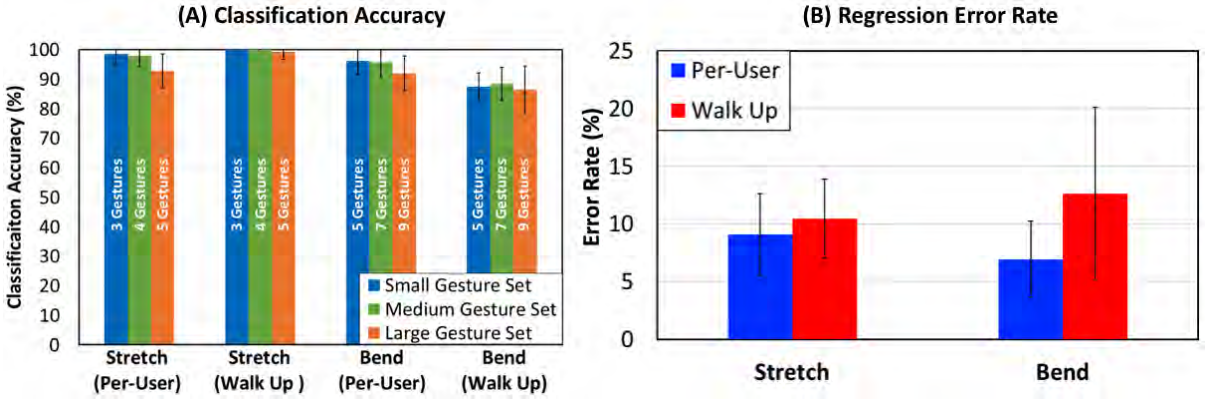

Fig. 14. Classification & regression accuracy: (A) Per-user (Real-time) and "Walk Up" (Post-hoc) classification accuracy for different numbers of stretch and bend gesture sets and (B) Per-user (Real-time) and "Walk Up" (Post-hoc) regression error rate for stretch and bend magnitude estimation.

In each fold, we only trained on 14 users' data and tested with the 15th user data which was never seen by the system.

Result: As shown in Figure 14(A), the per-user classification in real-time showed high accuracy overall. Even with the largest gesture set, the accuracy turned out to be 92.78% (SD=5.69) and 91.85% (SD=5.92) for stretch and bend, respectively. Unlike our expectation, we observed that the performance with "Stretch" increased to 99.19% (SD=2.58) for "Walk Up" accuracy. We presume that users exhibited a similar grasp, posture, and stretching magnitude during training. These physical similarities contributed to accumulating a similar set of sensor data for a robust classifier. "Walk Up" accuracy decreased an average of 7.13% for the bending deformation classification. We observed that bending had more flexibility for performing deformation, where points of inflection and supporting hand positions were different for each user. Still, the "Walk Up" classifier accuracy for nine bending gestures exceeded 87.45% (SD=4.60). This verifies that our system can easily be trained for individual users. Also, the "Walk Up" accuracy suggests that small amounts of data can be trained for use with a large number of users. When we only looked at reference gesture classifications, the average accuracy came out to be greater than 98% for both per-user and "Walk Up" classifications. The signal changes due to contacts (local deformation) yielded an order of magnitude less than that of stretch/bend (global deformation). Thus, it is hard to misclassify with non-reference gestures and this shows the robustness of employing deformation switch for various deformations.

8.3 Task 3: Regression Accuracy

We evaluated the regression accuracy in estimating the magnitude of the deformation. Similar to in **8.2**, we looked at the estimation error in 1) real-time per-user regression model, and 2) post-hoc analysis with the "Walk Up" regression model.

Setup: We followed the setup as in **8.2**. The only difference is that we trained for the magnitudes of the deformation using SVM regression. We devised the deformation into stretching and bending and recorded 0 to 5 levels of stretching and bending. Initially, we planned to train for the smallest and largest levels of deformations only to avoid the overfitting issue. During our preliminary experiment, however, we found that training with various magnitudes produced a more robust regression model. For "Stretch," we asked users to stretch up to 50% (Level 5) and each level was set at every 10%. For "Bend," we asked users to bend up to 150° (Level 5) for every

30°. We provided a physical stand with marked labels for participants to properly perform different levels of deformation (Figure 13(A) & (B)). Other than that, we did not give any specific guidance to participants. We asked users to hold the deformation at each different level for 1 *s*, and we captured the dataset which again consisted of 50 frames of raw sensor values. Then we proceeded with a regression classifier for estimating deformation levels. As in **Task 2**, we held a test session to evaluate the error rate of the regression model *live* with at least five trials for each level of deformation. We used a per-user classifier during the study and kept records of the sensor values to carry out a post-hoc analysis for the "Walk Up" error rate.

Result: We used an estimation error to evaluate the accuracy of the regression model. Upon the user's input, the SVM regression classifier put out float values ranging from 0~5. Then, we computed the error by comparing it to the ground truth (i.e., 0, 1, 2, 3, 4, and 5). Figure 14(B) shows the error rates for estimating the level of deformation. For the per-user regression model, the error rates were 9.09% (SD=3.53) and 6.93% (SD=3.31) for "Stretch" and "Bend," respectively. The error rates for "Walk Up" estimation were 10.45% (SD=3.41) for "Stretch" and 12.63% (SD=7.5) for "Bend". These results aligned with the findings from **8.2** where the freedom in performing gestures in "Bend" was more suitable for formulating an individual regression model with better accuracy. Still, all regression models achieved estimation errors of less than 12.63%, which can be interpreted as an average error at the 1.26 level for the range of 0~10 levels. This shows that the prototype is suitable for detecting the intensity of the deformation with instant training. Also, small amounts of trained data can be utilized for a large number of users.

8.4 User Feedback

In a post-survey, we elicited qualitative feedback about the participants' experience with the prototype. They reported enjoying the softness and rich sensing capability of the prototype, and they mentioned that the deformation was easy to perform since they often encountered this type of deformations in their everyday life. For improvements, participants recommended developing soft wires and electrodes to make all the components with soft materials. For potential applications, participants reported that the prototype would be a good fit for controlling digital devices with multimodal sensing features. The suggested form factors included gamepad, wristband, soft toys, phone case, etc. We demonstrate a few applications from these suggestions.

9 EXAMPLE APPLICATIONS

We demonstrate three applications that showcase the capabilities and interactions enabled by the real-time multimodal sensing. The following examples highlight the applicability in various environments with numerous form factors.

Stretchable Gamepad: Previously, a deformable gamepad was introduced utilizing discrete touch with bending deformation [17, 24, 35]. In this example, we implemented a stretchable gamepad where users can utilize

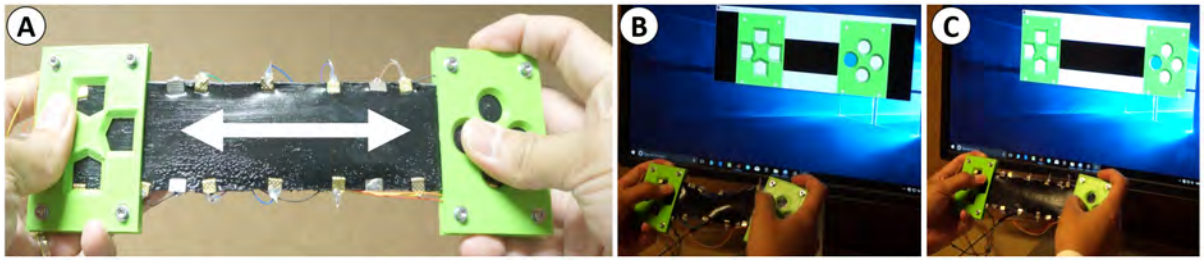

Fig. 15. Contact localization and stretching are embedded for utilizing natural human motions as input metaphors.

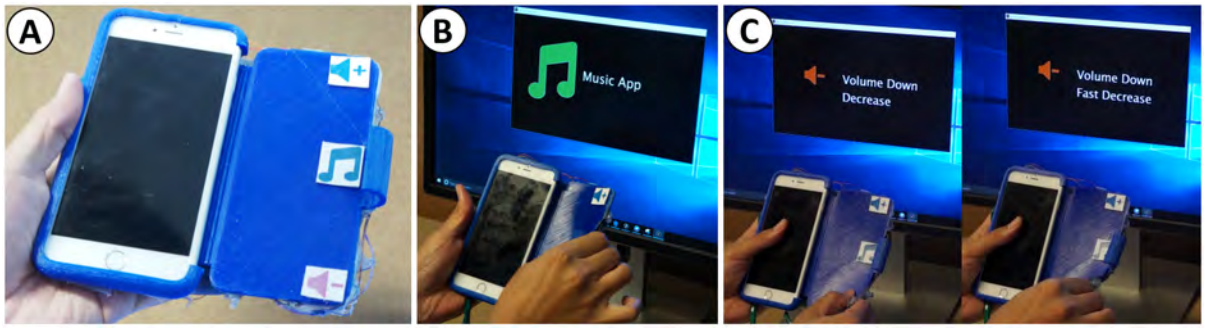

Fig. 16. The flip cover is embedded with bending gestures to provide discrete and continuous interactions.

stretching magnitude as an extra input in addition to discrete buttons. As shown in Figure 15, we inserted a single multilayer sensor with 20×5cm between 3D printed parts. We demonstrate how natural human motions can be exploited by introducing multimodal sensing.

Flexible Flip Cover: FlexCase [29] introduces an interactive flip cover utilizing grip and bend gestures. We made a flexible flip cover embedded with sensing bending in different locations and on different levels. The cover was made with semi-flexible material (TPU 95A) with the prototype was attached to the backside as shown in Figure 16. Users can simply bend in different locations to execute mapped applications. The level of bending can be used to control the intensity of the continuous control. We demonstrate the applicability of the prototype which can easily be attached to provide multimodal sensing capability to existing objects.

Wearable Input: We fabricated a wristband which is embedded with contact localization and different levels of the stretch as inputs. StretchEBand [43] demonstrated various applications utilizing the continuous stretch input. We further extended the interaction by merging two distinct sensing modalities. As shown in Figure 17, we showcase a wearable band that can be used with a smartwatch. Functions requiring secure interaction can be mapped with stretching input, which will produce fewer false triggers than contact sensing. A multi-level interaction is also possible with the multimodal sensing prototype, where users can 1) stretch the band to trigger the "Message Reply" function, 2) stretch the band using different levels to choose automated messages from the list, and 3) lift a contact finger on top to send a message. In this example, we demonstrate how rich inputs can be accomplished by utilizing multimodal sensing.

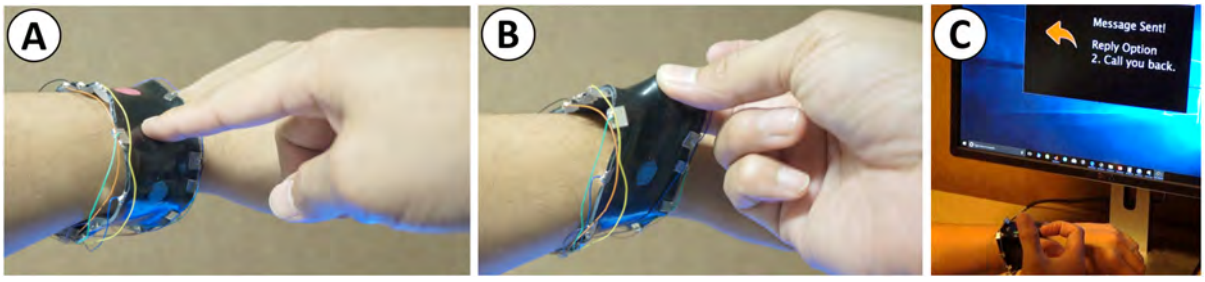

Fig. 17. A multi-level interaction is enabled with multimodal sensing with a wearable form factor.

Fig. 18. Fabrication via painting is possible using PDMS and a carbon elastomer mixture which can support 3D objects.

10 DISCUSSION AND LIMITATIONS

In the course of developing and testing *MultiSoft*, we identified several challenges and potential findings for improvements. We discuss these along with future works.

Alternative Fabrication Method: We introduce a multilayer sensor structure in this chapter. Although not fully developed, we tested and saw potential in mixing PDMS with a carbon elastomer. With a ratio greater than 5:1 (PDMS:carbon elastomer), the sensor can be cured under 70° for 10 minutes. With further investigation, we can make a soft interactive agent that can be painted on any 3D object as shown in Figure 18.

Electrode Connection & Placement: The high flexibility and stretchability of the prototype produce signal noises due to the physical fluctuation on the attached hard wires and electrodes. In the future, we plan to employ a stretchable conductive wire [5] which can possibly replace the existing rigid components.

In our work, electrodes were evenly placed around the sensing region. However, this electrode configuration reduces the flexibility in design since physical electrodes need to be placed all around the region. As demonstrated in a previous work [2], it is in our interest to test distinct electrode configuration setups.

Scalability & Form Factor: In the current lab environment, the scalable size and fabrication uniformity of the sensor is limited due to the size of the molds and the surface roughness during manual painting, etc. In this study, we have made over >10 different samples and used 1~2 samples for each the test. In our future work, this limitation can be overcome with advanced manufacturing setups such as multi-stage extrusion [12, 18]. The current form factor is also limited in terms of 2D sheets. Recent developments in carbon nanotube related fabrication [34] show potential for the 3D printing of soft sensors. Thus, it is within our interest to explore further the feasibility of making a 3D printable soft sensor.

We currently support the ad-hoc training approach for recognizing deformations. The change in the electrode placement and the sensor size would require retraining of SVM. In the future, we will emphasize the training with deep learning models corresponding to various types of geometry. We can perform the learning process with synthesized sensor values obtained from solving the forward problem in EIT.

Improving Sensing Performance: The employed capacitive sensing or dynamic manipulation calibration do not indicate the material's viscoelastic response. As long as sufficient deformations happen, however, both the contact localization and deformation sensing work robustly for periodic interactions. We confirmed that there is no performance degradation unless users repeatedly contact or bend/stretch the same location at a high frequency (> 5 Hz), which usually is not the case for common interactions.

From the result in **8.1**, we suggested that holding a few frames before re-initiating the localization and after releasing the deformation would improve the accuracy. We tested with three users by applying a fixed duration of hold (1.5*s*) on the recorded sensor data. On average, we observed about 20% improvement in accuracy. It is possible to further improve an accuracy with optimized delay according to different types and magnitudes of deformations.

As shown in our evaluation results, a deformation involving more freedom in execution often leads to a worse performance. To provide robust interactions, we recommend offering a set of general guidelines for the HCI designer on how to perform the deformation. In this way, the accuracy of the classification and the estimation of the deformation can be improved.

11 CONCLUSION

We propose a multilayer soft sensor capable of sensing localization and deformation. With the proposed multimodal sensing pipeline, we enable a real-time contact localization, deformation classification, and estimation of deformation levels. By introducing a dynamic manipulation and a deformation switch, contact localization can be maintained in the presence of deformation. We also introduce a multilayer sensor structure with high flexibility and stretchability to reduce the sensor settlement duration. We confirmed the system accuracy and performance with real users through per-user and "Walk Up" classifications. Our work will bring about expanded interactions through multimodal sensing capability for future input metaphors.

ACKNOWLEDGMENTS

We thank the reviewers for their valuable feedback and comments. This work was supported partially by the NSF Award #1637961 (NRI). We also acknowledge the Feddersen chair and Engineering Faculty Conversations (EFC) Deans Funding for Future of Work. Any opinions, findings, and conclusions or recommendations expressed in this material are those of the author(s) and do not necessarily reflect the views of the National Science Foundation.

REFERENCES

[1] Andy Adler and Robert Guardo. 1996. Electrical impedance tomography: regularized imaging and contrast detection. *IEEE Transactions on Medical Imaging* 15, 2 (Apr 1996), 170–179. http://doi.org/10.1109/42.491418

[2] Hassan Alirezaei, Akihiko Nagakubo, and Yasuo Kuniyoshi. 2007. A highly stretchable tactile distribution sensor for smooth surfaced humanoids. In *2007 7th IEEE-RAS International Conference on Humanoid Robots*. 167–173. http://doi.org/10.1109/ICHR.2007.4813864

[3] Hassan Alirezaei, Akihiko Nagakubo, and Yasuo Kuniyoshi. 2009. A tactile distribution sensor which enables stable measurement under high and dynamic stretch. In *3D User Interfaces, 2009. 3DUI 2009. IEEE Symposium on*. IEEE, 87–93.

[4] B H Brown and A D Seagar. 1987. The Sheffield data collection system. *Clinical Physics and Physiological Measurement* 8, 4A (1987), 91. http://stacks.iop.org/0143-0815/8/i=4A/a=012

[5] Tao Chen, Rui Hao, Huisheng Peng, and Liming Dai. 2015. High-Performance, Stretchable, Wire-Shaped Supercapacitors. *Angewandte Chemie International Edition* 54, 2 (2015), 618–622. http://dx.doi.org/10.1002/anie.201409385

[6] Jingyuan Cheng, Mathias Sundholm, Bo Zhou, Marco Hirsch, and Paul Lukowicz. 2016. Smart-surface: Large scale textile pressure sensors arrays for activity recognition. *Pervasive and Mobile Computing* 30 (2016), 97–112.

[7] Jingyuan Cheng, Bo Zhou, Kai Kunze, Carl Christian Rheinländer, Sebastian Wille, Norbert Wehn, Jens Weppner, and Paul Lukowicz. 2013. Activity recognition and nutrition monitoring in every day situations with a textile capacitive neckband. In *Proceedings of the 2013 ACM conference on Pervasive and ubiquitous computing adjunct publication*. ACM, 155–158.

[8] Chin-yu Chien, Rong-Hao Liang, Long-Fei Lin, Liwei Chan, and Bing-Yu Chen. 2015. FlexiBend: Enabling Interactivity of Multi-Part, Deformable Fabrications Using Single Shape-Sensing Strip. In *Proceedings of the 28th Annual ACM Symposium on User Interface Software & Technology (UIST '15)*. ACM, New York, NY, USA, 659–663. http://doi.acm.org/10.1145/2807442.2807456

[9] Jean-Baptiste Chossat, Hee-Sup Shin, Yong-Lae Park, and Vincent Duchaine. 2015. Soft tactile skin using an embedded ionic liquid and tomographic imaging. *Journal of Mechanisms and Robotics* 7, 2 (2015), 021008. http://doi.org10.1115/1.4029474

[10] Artem Dementyev and Joseph A. Paradiso. 2014. WristFlex: Low-power Gesture Input with Wrist-worn Pressure Sensors. In *Proceedings of the 27th Annual ACM Symposium on User Interface Software and Technology (UIST '14)*. ACM, New York, NY, USA, 161–166. http://doi.org/10.1145/2642918.2647396

[11] Sean Follmer, Daniel Leithinger, Alex Olwal, Nadia Cheng, and Hiroshi Ishii. 2012. Jamming User Interfaces: Programmable Particle Stiffness and Sensing for Malleable and Shape-changing Devices. In *Proceedings of the 25th Annual ACM Symposium on User Interface Software and Technology (UIST '12)*. ACM, New York, NY, USA, 519–528. http://doi.org/10.1145/2380116.2380181

[12] B. Hagström, A. LUND, and E. Nilsson. 2014. Method of producing a piezoelectric and pyroelectric fiber. (Oct. 9 2014). WO Patent App. PCT/EP2014/056,658.

[13] Mark Hall, Eibe Frank, Geoffrey Holmes, Bernhard Pfahringer, Peter Reutemann, and Ian H. Witten. 2009. The WEKA Data Mining Software: An Update. *SIGKDD Explor. Newsl.* 11, 1 (Nov. 2009), 10–18. http://doi.acm.org/10.1145/1656274.1656278

[14] John-Erik Haugen, Oliver Tomic, and Knut Kvaal. 2000. A calibration method for handling the temporal drift of solid state gas-sensors. *Analytica Chimica Acta* 407, 1 (2000), 23–39. https://doi.org/10.1016/S0003-2670(99)00784-9

[15] PJRC Inc. 2017. Product Detail. (2017). Retrieved November 1, 2017 from http://www.pjrc.com/teensy/index.html.

[16] Hsin-Liu (Cindy) Kao, Christian Holz, Asta Roseway, Andres Calvo, and Chris Schmandt. 2016. DuoSkin: Rapidly Prototyping On-skin User Interfaces Using Skin-friendly Materials. In *Proceedings of the 2016 ACM International Symposium on Wearable Computers (ISWC '16)*. ACM, New York, NY, USA, 16–23. http://doi.acm.org/10.1145/2971763.2971777

[17] Johan Kildal, Susanna Paasovaara, and Viljakaisa Aaltonen. 2012. Kinetic Device: Designing Interactions with a Deformable Mobile Interface. In *CHI '12 Extended Abstracts on Human Factors in Computing Systems (CHI EA '12)*. ACM, New York, NY, USA, 1871–1876. DOI: http://dx.doi.org/10.1145/2212776.2223721

[18] A. KÖLLNBERGER and A. Schwinghammer. 2014. Production of thin silicone films. (June 19 2014). WO Patent App. PCT/EP2013/073,914.

[19] Gierad Laput, Eric Brockmeyer, Scott E. Hudson, and Chris Harrison. 2015. Acoustruments: Passive, Acoustically-Driven, Interactive Controls for Handheld Devices. In *Proceedings of the 33rd Annual ACM Conference on Human Factors in Computing Systems (CHI '15)*. ACM, New York, NY, USA, 2161–2170. http://doi.acm.org/10.1145/2702123.2702414

[20] Gierad Laput, Yang Zhang, and Chris Harrison. 2017. Synthetic Sensors: Towards General-Purpose Sensing. In *Proceedings of the 2017 CHI Conference on Human Factors in Computing Systems (CHI '17)*. ACM, New York, NY, USA, 3986–3999. http://doi.acm.org/10.1145/3025453.3025773

[21] Hyosang Lee, Donguk Kwon, Haedo Cho, Inkyu Park, and Jung Kim. 2017. Soft Nanocomposite Based Multi-point, Multi-directional Strain Mapping Sensor Using Anisotropic Electrical Impedance Tomography. *Scientific reports* 7 (2017). http://doi.org/10.1038/srep39837

[22] Joanne Leong, Patrick Parzer, Florian Perteneder, Teo Babic, Christian Rendl, Anita Vogl, Hubert Egger, Alex Olwal, and Michael Haller. 2016. proCover: Sensory Augmentation of Prosthetic Limbs Using Smart Textile Covers. In *Proceedings of the 29th Annual Symposium on User Interface Software and Technology (UIST '16)*. ACM, New York, NY, USA, 335–346. http://doi.org/10.1145/2984511.2984572

[23] F. Lorussi, Enzo Pasquale Scilingo, M. Tesconi, A. Tognetti, and D. De Rossi. 2005. Strain sensing fabric for hand posture and gesture monitoring. *IEEE Transactions on Information Technology in Biomedicine* 9, 3 (Sept 2005), 372–381. http://doi.org/10.1109/TITB.2005.854510

[24] Vinh P. Nguyen, Sang Ho Yoon, Ansh Verma, and Karthik Ramani. 2014. BendID: Flexible Interface for Localized Deformation Recognition. In *Proceedings of the 2014 ACM International Joint Conference on Pervasive and Ubiquitous Computing (UbiComp '14)*. ACM, New York, NY, USA, 553–557. http://doi.acm.org/10.1145/2632048.2636092

[25] Patrick Parzer, Adwait Sharma, Anita Vogl, Jürgen Steimle, Olwal Alex, and Michael Haller. 2017. SmartSleeve: Real-time Sensing of Surface and Deformation Gestures on Flexible, Interactive Textiles, using a Hybrid Gesture Detection Pipeline. In *Proceedings of the 30th Annual ACM Symposium on User Interface Software & Technology (UIST '17)*. ACM, New York, NY, USA, 565–577. http://doi.acm.org/10.1145/3126594.3126652

[26] Ivan Poupyrev, Nan-Wei Gong, Shiho Fukuhara, Mustafa Emre Karagozler, Carsten Schwesig, and Karen E Robinson. 2016. Project Jacquard: interactive digital textiles at scale. In *Proceedings of the 2016 CHI Conference on Human Factors in Computing Systems*. ACM, 4216–4227.

[27] Gonzalo Ramos, Matthew Boulos, and Ravin Balakrishnan. 2004. Pressure Widgets. In *Proceedings of the SIGCHI Conference on Human Factors in Computing Systems (CHI '04)*. ACM, New York, NY, USA, 487–494. http://doi.org/10.1145/985692.985754

[28] Christian Rendl, David Kim, Sean Fanello, Patrick Parzer, Christoph Rhemann, Jonathan Taylor, Martin Zirkl, Gregor Scheipl, Thomas Rothländer, Michael Haller, and Shahram Izadi. 2014. FlexSense: A Transparent Self-sensing Deformable Surface. In *Proceedings of the 27th Annual ACM Symposium on User Interface Software and Technology (UIST '14)*. ACM, New York, NY, USA, 129–138. http://doi.acm.org/10.1145/2642918.2647405

[29] Christian Rendl, David Kim, Patrick Parzer, Sean Fanello, Martin Zirkl, Gregor Scheipl, Michael Haller, and Shahram Izadi. 2016. FlexCase: Enhancing Mobile Interaction with a Flexible Sensing and Display Cover. In *Proceedings of the 2016 CHI Conference on Human Factors in Computing Systems (CHI '16)*. ACM, New York, NY, USA, 5138–5150. http://doi.acm.org/10.1145/2858036.2858314

[30] Peter Roberts, Dana D. Damian, Wanliang Shan, Tong Lu, and Carmel Majidi. 2013. Soft-matter capacitive sensor for measuring shear and pressure deformation. In *2013 IEEE International Conference on Robotics and Automation*. 3529–3534. http://doi.org/10.1109/ICRA.2013.6631071

[31] Munehiko Sato, Ivan Poupyrev, and Chris Harrison. 2012. Touché: Enhancing Touch Interaction on Humans, Screens, Liquids, and Everyday Objects. In *Proceedings of the SIGCHI Conference on Human Factors in Computing Systems (CHI '12)*. ACM, New York, NY, USA, 483–492. http://doi.acm.org/10.1145/2207676.2207743

[32] Munehiko Sato, Rohan S. Puri, Alex Olwal, Yosuke Ushigome, Lukas Franciszkiewicz, Deepak Chandra, Ivan Poupyrev, and Ramesh Raskar. 2017. Zensei: Embedded, Multi-electrode Bioimpedance Sensing for Implicit, Ubiquitous User Recognition. In *Proceedings of the 2017 CHI Conference on Human Factors in Computing Systems (CHI '17)*. ACM, New York, NY, USA, 3972–3985. http://doi.acm.org/10.1145/3025453.3025536

[33] Martin Schmitz, Jürgen Steimle, Jochen Huber, Niloofar Dezfuli, and Max Mühlhäuser. 2017. Flexibles: Deformation-Aware 3D-Printed

Tangibles for Capacitive Touchscreens. In *Proceedings of the 2017 CHI Conference on Human Factors in Computing Systems (CHI '17)*. ACM, New York, NY, USA, 1001–1014. http://doi.acm.org/10.1145/3025453.3025663

[34] Su Ryon Shin, Raziyeh Farzad, Ali Tamayol, Vijayan Manoharan, Pooria Mostafalu, Yu Shrike Zhang, Mohsen Akbari, Sung Mi Jung, Duckjin Kim, Mattia Comotto, Nasim Annabi, Faten Ebrahim Al-Hazmi, Mehmet R. Dokmeci, and Ali Khademhosseini. 2016. A Bioactive Carbon Nanotube-Based Ink for Printing 2D and 3D Flexible Electronics. *Advanced Materials* 28, 17 (2016), 3280–3289. DOI: http://dx.doi.org/10.1002/adma.201506420

[35] Paden Shorey and Audrey Girouard. 2017. Bendtroller:: An Exploration of In-Game Action Mappings with a Deformable Game Controller. In *Proceedings of the 2017 CHI Conference on Human Factors in Computing Systems (CHI '17)*. ACM, New York, NY, USA, 1447–1458. http://doi.acm.org/10.1145/3025453.3025463

[36] David Silvera Tawil, David Rye, and Mari Velonaki. 2012. Interpretation of the modality of touch on an artificial arm covered with an EIT-based sensitive skin. *The International Journal of Robotics Research* 31, 13 (2012), 1627–1641.

[37] Ronit Slyper, Ivan Poupyrev, and Jessica Hodgins. 2011. Sensing Through Structure: Designing Soft Silicone Sensors. In *Proceedings of the Fifth International Conference on Tangible, Embedded, and Embodied Interaction (TEI '11)*. ACM, New York, NY, USA, 213–220. http://doi.acm.org/10.1145/1935701.1935744

[38] Smooth-On. 2017. Ecoflex. (2017). Retrieved November 1, 2017 from https://www.smooth-on.com/products/.

[39] Yuta Sugiura, Masahiko Inami, and Takeo Igarashi. 2012. A Thin Stretchable Interface for Tangential Force Measurement. In *Proceedings of the 25th Annual ACM Symposium on User Interface Software and Technology (UIST '12)*. ACM, New York, NY, USA, 529–536. http://doi.acm.org/10.1145/2380116.2380182

[40] Mahmoud Tavakoli, Rui Rocha, Luis Osorio, Miguel Almeida, Anibal de Almeida, Vivek Ramachandran, Arya Tabatabai, Tong Lu, and Carmel Majidi. 2017. Carbon doped PDMS: conductance stability over time and implications for additive manufacturing of stretchable electronics. *Journal of Micromechanics and Microengineering* 27, 3 (2017), 035010. http://stacks.iop.org/0960-1317/27/i=3/a=035010

[41] Karen Vanderloock, Vero Vanden Abeele, Johan A.K. Suykens, and Luc Geurts. 2013. The Skweezee System: Enabling the Design and the Programming of Squeeze Interactions. In *Proceedings of the 26th Annual ACM Symposium on User Interface Software and Technology (UIST '13)*. ACM, New York, NY, USA, 521–530. http://doi.org/10.1145/2501988.2502033

[42] M Vauhkonen, W R B Lionheart, L M Heikkinen, P J Vauhkonen, and J P Kaipio. 2001. A MATLAB package for the EIDORS project to reconstruct two-dimensional EIT images. *Physiological Measurement* 22, 1 (2001), 107. http://stacks.iop.org/0967-3334/22/i=1/a=314

[43] Anita Vogl, Patrick Parzer, Teo Babic, Joanne Leong, Alex Olwal, and Michael Haller. 2017. StretchEBand: Enabling Fabric-based Interactions Through Rapid Fabrication of Textile Stretch Sensors. In *Proceedings of the 2017 CHI Conference on Human Factors in Computing Systems (CHI '17)*. ACM, New York, NY, USA, 2617–2627. http://doi.acm.org/10.1145/3025453.3025938

[44] Wacker. 2017. ELASTOSIL LR 3162 A/B. (2017). Retrieved November 1, 2017 from https://www.wacker.com.

[45] Martin Weigel, Tong Lu, Gilles Bailly, Antti Oulasvirta, Carmel Majidi, and Jürgen Steimle. 2015. iSkin: Flexible, Stretchable and Visually Customizable On-Body Touch Sensors for Mobile Computing. In *Proceedings of the 33rd Annual ACM Conference on Human Factors in Computing Systems (CHI '15)*. ACM, New York, NY, USA, 2991–3000. http://doi.org/10.1145/2702123.2702391

[46] Martin Weigel, Aditya Shekhar Nittala, Alex Olwal, and Jürgen Steimle. 2017. SkinMarks: Enabling Interactions on Body Landmarks Using Conformal Skin Electronics. In *Proceedings of the 2017 CHI Conference on Human Factors in Computing Systems (CHI '17)*. ACM, New York, NY, USA, 3095–3105. http://doi.acm.org/10.1145/3025453.3025704

[47] Michael Wessely, Theophanis Tsandilas, and Wendy E. Mackay. 2016. Stretchis: Fabricating Highly Stretchable User Interfaces. In *Proceedings of the 29th Annual Symposium on User Interface Software and Technology (UIST '16)*. ACM, New York, NY, USA, 697–704. http://doi.org/10.1145/2984511.2984521

[48] Sang Ho Yoon, Ke Huo, Vinh P. Nguyen, and Karthik Ramani. 2015. TIMMi: Finger-worn Textile Input Device with Multimodal Sensing in Mobile Interaction. In *Proceedings of the Ninth International Conference on Tangible, Embedded, and Embodied Interaction (TEI '15)*. ACM, New York, NY, USA, 269–272. http://doi.org/10.1145/2677199.2680560

[49] Sang Ho Yoon, Ke Huo, Yunbo Zhang, Guiming Chen, Luis Paredes, Subramanian Chidambaram, and Karthik Ramani. 2017. iSoft: A Customizable Soft Sensor with Real-time Continuous Contact and Stretching Sensing. In *Proceedings of the 30th Annual ACM Symposium on User Interface Software & Technology (UIST '17)*. ACM, New York, NY, USA, 665–678. http://doi.acm.org/10.1145/3126594.3126654

[50] Yang Zhang, Gierad Laput, and Chris Harrison. 2017. Electrick: Low-Cost Touch Sensing Using Electric Field Tomography. In *Proceedings of the 2017 CHI Conference on Human Factors in Computing Systems (CHI '17)*. ACM, New York, NY, USA, 1–14. http://doi.org/10.1145/3025453.3025842

[51] Yang Zhang, Robert Xiao, and Chris Harrison. 2016. Advancing Hand Gesture Recognition with High Resolution Electrical Impedance Tomography. In *Proceedings of the 29th Annual Symposium on User Interface Software and Technology (UIST '16)*. ACM, New York, NY, USA, 843–850. http://doi.acm.org/10.1145/2984511.2984574

Received February 2018; revised May 2018; accepted September 2018